Ecotoxicology and Environmental Safety 226 (2021) 112868

Contents lists available at ScienceDirect

Ecotoxicology and Environmental Safety

journal homepage: www.elsevier.com/locate/ecoenv

Metal tolerance protein MTP6 is involved in Mn and Co distribution in poplar

Fengming Yang [a], Yongfeng Gao [a,*], Jikai Liu [a], Zihao Chen [a], Víctor Resco de Dios [a,b], Qian Gao [a], Meng Zhang [a], Zhuoxi Peng [a], Yinan Yao [a,*]

[a] School of Life Science and Engineering, Southwest University of Science and Technology, Mianyang 621010, China
[b] Department of Crop and Forest Sciences & Joint Research Unit CTFC-AGROTECNIO-CERCA Center, Universitat de Lleida, 25198 Lleida, Spain

ARTICLE INFO

Edited by Dr. Fernando Barbosa

Keywords:
metal tolerance protein
pre-vacuolar compartment
manganese
cobalt
metal distribution
poplar

ABSTRACT

With the booming demand of the electric vehicle industry, the concentration of manganese (Mn) and cobalt (Co) flowing into land ecosystems has also increased significantly. While these transition metals can promote the growth and development of plants, they may become toxic under high concentrations. It is thus important to understand how Mn and Co are distributed in plants to develop novel germplasms for the remediation of these heavy metals in contaminated soils. Here, an *MTP* gene that encodes the CDF (cation diffusion facilitator) protein in *Populus trichocarpa*, *PtrMTP6,* was screened as the key gene involved in the distribution of both Mn and Co in poplar. The PtrMTP6-GFP fusion protein was co-localized with the mRFP-VSR2, showing that PtrMTP6 proteins are present at the pre-vacuolar compartment (PVC). Yeast mutant complementation assays further identified that PtrMTP6 serves as a Mn and Co transporter, reducing yeast cell toxicity after exposure to excessive Mn or Co. Histochemical analyses showed that *PtrMTP6* was mainly expressed in phloem, suggesting that PtrMTP6 probably involved in the Mn and Co transport via phloem in plants. Under excess Co, PtrMTP6 overexpressing poplar lines were more severely damaged than the control due to higher Co accumulations in young tissue. PtrMTP6 overexpressing lines showed little change in their tolerance to excess Mn, although young tissues also accumulated more Mn. PtrMTP6 play important roles in Mn and Co distribution in poplar and further research on its regulation will be important to increase bioremediation in Mn and Co polluted ecosystems.

1. Introduction

Some of transitional elements such as Manganese (Mn) and Cobalt (Co) are widely involved in the plant growth and development. Manganese plays a well-known role in photosynthesis, where it participates in the water-splitting process at the PSII reaction center with the Mn_4Ca cluster (Umena et al., 2011). Mn also serves as an activator of many different enzymes, such as superoxide dismutase (Mn-SOD) and oxalate oxidases, which are involved in the detoxification of reactive oxygen species (ROS) (Abreu and Cabelli, 2010). Mn is also involved in glycosyl transferases, decarboxylases, and dehydrogenases amongst others (Andresen et al., 2018; Del Rio et al., 1983; Woo et al., 2000). Cobalt is mainly found in the cobalamin (vitamin B12) (Banerjee and Ragsdale, 2003). Additionally, Co is also present, without the corrin ring of B_{12}, in some proteins like methionine aminopeptidase, prolidase, and nitrile hydratase, although these are not Co-specific proteins (Kobayashi and Shimizu, 1999).

Although Manganese and Cobalt are involved in plant metabolism, they are toxic when present in excess (Kramer, 2010). At poorly-aerated or acid soils, for instance, the absorption of Mn may exceed plant requirements. The first effect of Mn toxicity is growth inhibition (Eroglu et al., 2016; Peiter et al., 2007; Zhao et al., 2017). Increasing Mn toxicity then leads to leaf or interveinal chlorosis and necroses, due to the obstruction of chlorophyll biosynthesis and PSI photochemistry (Gonz et al., 1999; Horst et al., 1999; Millaleo et al., 2013). Regarding cobalt toxicity, excess Co leads to vein discolor, green inhibition, leaf fall, and shoot weight reduce. This is because Co toxicity damages the plastids and inhibits the PSII, and it interrupts the processes of karyokinesis and cytokinesis (Mohanty et al., 1989; Palit et al., 1994).

Global demands of manganese (Mn) and cobalt (Co) are expected to increase five- to ten-fold by 2030, due to the booming electric vehicle industry (Deetman et al., 2018; Habib et al., 2020). These increases in mining for Mn and Co are likely to lead to increases their concentrations in soils. These two metals are participating in the plant growth and

* Corresponding authors.
E-mail addresses: gaoyongfeng0263@swust.edu.cn (Y. Gao), yinanyao@swust.edu.cn (Y. Yao).

https://doi.org/10.1016/j.ecoenv.2021.112868
Received 28 June 2021; Received in revised form 27 September 2021; Accepted 1 October 2021
Available online 4 October 2021

development, but they may become toxic under high concentrations (Kramer, 2010). It is thus important to develop novel germplasms for the remediation of contaminated ecosystems with high concentrations of Mn and Co.

Plants usually use diverse mechanisms to cope with metal toxicity, and one of them is the preferential allocation of heavy metals to old, instead of young tissues. Additionally, cellular detoxification mechanisms often involve the storage of heavy metals in compartments like the vacuole or the apoplast, which is achieved by transport proteins. Many heavy metal transporters have been characterized, like those in families Nramp, IRT, and MTP. Some cobalt transporters have been identified in yeast and in lower plants, like COT1 in Saccharomyces cerevisiae (Conklin et al., 1992), CrNRAMP1 in Chlamydomonas reinhardtii (Chang et al., 2020). However, cobalt transporters in higher plants are largely unknown so far.

In recent years, poplars have been proposed for phytoremediation due to the high above-ground biomass, highly branched root system, fast growth, effectively absorb heavy metals and translocation to the above-ground parts (Di Lonardo et al., 2011; Fischerová et al., 2006; Laureysens et al., 2005; Pietrini et al., 2009; Unterbrunner et al., 2007). In addition, some species of poplars can also accumulate heavy metals close to the threshold value of hyperaccumulators (He et al., 2013, 2011). Akkus Ozen and Yaman (2017) reported that poplars (Populus nigra L.) are cobalt hyperaccumulators, as they show no visible symptoms with concentrations as high as 2.07 mg Kg^{-1} (that concentrations in Morus L. and Robinia pseudoacacia L. only 0.31 mg Kg^{-1} or 0.22 mg Kg^{-1} in same environment). Poplars could thus be well suited for bioremediation of ecosystems affected by the battery production and electric vehicle industry. However, the mechanisms underlying the translocation capacity in Co are currently unknown.

Using the yeast functional complementation method, we have previously screened a transporter from large MTP families in Populus trichocarpa, PtrMTP6, which confers Mn and Co tolerance (Gao et al., 2020) (The Fe hardly be toxic to living being, thus we focus in Mn and Co although MTP6 seems also effect on Fe tolerance in yeast). We therefore hypothesized that PtrMTP6 would also involve in transport of Mn and Co in poplar. To test this hypothesis, we further investigated the biological function of PtrMTP6 by analyzing the following: its expression pattern in different organs of wild type poplar; GUS histochemical staining in different organs of transgenic poplar; PtrMTP6 subcellular localization in rice mesophyll protoplasts; and the effects of *PtrMTP6* expression on Mn and Co tolerance and accumulation in yeast and on Mn and Co transport properties in poplar.

2. Materials and methods

2.1. Plant material and growth conditions

We grew test-tube plantets of *Populus trichocarpa* Torr. & Gray and *Populus tomentosa* Carr. clone 741 in woody plant medium (WPM) containing 30 g/L sucrose and 0.6% (w/v) agar, with the pH adjusted at 5.85 (Lloyd and Mccown, 1980). The plants were grown in the greenhouse at 24 °C with 16 h/8 h light (4500 lx)/dark cycle. After three weeks, the rooted plants were transferred and cultivated as hydroponics (Hoagland and Arnon, 1950). Plants were grown in the greenhouse using half strength Hoagland nutrient solution (pH 6.0) under a photoperiod of 16 h/8 h (day/night) and temperatures of 24 °C/18 °C.

2.2. Cloning PtrMTP6 and sequence analyses

Total RNA was extracted from 8-weeks-old *Populus trichocarpa* Torr. & Gray plants using RNAprep Pure Plant Kit (Polysaccharides & Polyphenolics-rich RNAprep Pure, Tiangen, China). Subsequently, 2 μg of total RNA were used for cDNA synthesis using the first-strand cDNA Synthesis Kit (ProbeGene, China). The specific primers (PtrMTP6-F0 and PtrMTP6-R0, see Table S1) for PCR were designed by Primer Premier 5, based on the reference sequence downloaded from NCBI (https://www.ncbi.nlm.nih.gov/, XM_006386701). After the PCR reaction, the targeted fragments were cloned into the pEASY-Blunt vector (TransGen Biotech, China) for sequencing.

We downloaded predicted homologous amino acid sequences of PtrMTP6 (based on results for other species) from Phytozome (https://phytozome.jgi.doe.gov/pz/portal.html). Those included AtMTP6, CsMTP6, OsMTP6, VvMTP6 and ZmMTP6 (Gao et al., 2020). DNAMAN software was used to perform the multiple sequence alignments. The transmembrane topology of PtrMTP6 was predicted using CCTOP (http://cctop.enzim.ttk.mta.hu/) (Dobson et al., 2015) and visualized by TMRPres2D (Spyropoulos et al., 2004). The InterPro website (http://www.ebi.ac.uk/interpro/) (Blum et al., 2021) was used for conserved domain analyses.

2.3. Yeast expression, growth curve, and metal content assay

The full coding region of *PtrMTP6* was amplified from cDNA using the gene specific primers PtrMTP6-F1 and PtrMTP6-R1 (Table S1). The PCR product was cloned into the pYES2.0 vector to yield the recombinant plasmid pYES2.0-*PtrMTP6*. Yeast (Saccharomyces cerevisiae) strains were obtained from Euroscarf (http://www.euroscarf.de/), including Y00000 (BY4741), Y04534 (Δ*pmr1*) and Y01613 (Δ*cot1*). Then, the recombinant plasmid pYES2.0-*PtrMTP6* was transformed into the above yeast strain cells using the LiOAc/PEG method (Gietz and Schiestl, 2007). The transformed colonies were plated on SD/Glu-Ura (synthetic defined medium without Uracil), which contains different concentrations of Co and Mn, and we then measured yeast growth.

We developed a yeast growth curve assay, where transformed yeast cells pre-cultured in 5 mL SD/Glu-Ura growing medium were shaken at 200 rpm and 30 °C overnight, until reaching the growth exponential phase ($OD_{600} \approx 0.4$). The OD_{600} of the pre-cultures was then adjusted to 0.4, and 500 μL of the pre-cultures were inoculated into 20 mL SD/Gal-Ura growing medium containing either 10 mM $MnSO_4$ or 1 mM $CoCl_2$, respectively ($n = 3$). Cultures were grown in a shaker at 200 rpm and 30 °C, and the OD_{600} values were measured every 12 h during 3 days.

We then assessed Mn and Co accumulation in yeast cells using the same growing methods as in the growth curve assays described previously. 500 μL pre-cultures ($OD_{600} = 0.4$) were inoculated into 50 mL of the SD/Gal-Ura growing medium, and grown at 30 °C in shaker with 200 rpm for 12 h. We then added the different metals into the cultures until we reached either 5 mM $MnSO_4$ or 0.5 mM $CoCl_2$, respectively, and allowed growth for 6 h. The yeast cells were then collected from the centrifuge (6000 rpm, 5 min) and washed by 10 mM EDTA-2Na and deionized H_2O three times. The yeast collections were dried in the oven at 65 °C for 3 days. After drying, the yeast cells were digested with concentrated HNO_3 (65%) at 160 °C for 1 h. Then the samples were diluted to 25 mL using deionized H_2O. Mn and Co contents in yeast were measured using flame atomic absorption spectrometry (AAS, PerkinElmer, United States).

2.4. Quantitative RT-PCR and GUS staining

Different organs (including roots, stems, shoot apex, axillary buds, mature leaves, young leaves, and petioles) of 8-weeks old *Populus trichocarpa* plants were used for total RNA extraction and reverse transcription into cDNA. Quantitative RT-PCR analyses of *PtrMTP6* (qRT-PtrMTP6-F and qRT-PtrMTP6-R, Table S1) were performed with the TransStart Green qPCR SuperMix (TransGen Biotech, China) in 96-well plates using the CFX96 Real-Time System (Bio-Rad, United States). Two house-keeping genes *UBQ* (GenBank accession LOC7455401) and *EF1α* (GenBank accession LOC18100225) were used as internal references. The relative expression values were determined against the control sample by using the $2^{-\Delta\Delta Ct}$ method (Livak and Schmittgen, 2001).

We used the genomic DNA of *Populus trichocarpa* for amplifying the *PtrMTP6* gene promoter through specific primers (Pro-PtrMTP6-F0, Pro-

PtrMTP6-R0, Pro-PtrMTP6-F1, and Pro-PtrMTP6-R1; Table S1). The PtrMTP6 promoter DNA fragment contained 2051 bp upstream the *PtrMTP6* start codon and it was cloned into the pBI121 vector to drive the expression of the *GUS* reporter gene (pBI121-*PtrMTP6*$_{pro}$*::GUS*). Then, we introduced the recombinant plasmid into *Agrobacterium tumefaciens* strain EHA105, and we further transformed the wild type *Populus tomentosa*. Histochemical analyses of transgenic poplars with expression of *PtrMTP6*$_{pro}$*::GUS* were performed following previous protocols (Jefferson, 1987). Various fresh organs and sections of the 8-weeks-old transgenic plants were incubated into the GUS staining buffer at 37 °C overnight, and then subjected to ethanol for decolorize. Stained organs or sections were visualized using a Leica microscope (Leica MDG33/10450123, Leica microsystems Inc.).

2.5. Subcellular localization

For the construction of the fusion expression vector pTEX-*35S*$_{pro}$*::PtrMTP6-GPF*, the full length of the coding sequence (CDS) without the termination codon of *PtrMTP6* was amplified by using gene-specific primers (GFP-PtrMTP6-F1 and GFP-PtrMTP6-R1, Table S1). The fragments were then cloned into the pTEX-*GFP* vector. The separation and transformation of protoplasts were performed as described previously (Li et al., 1990). The fusion expression vector pTEX-*35S*$_{pro}$*::PtrMTP6-GPF* was used for observing the localization of the PtrMTP6 protein in *Oryza sativa* protoplast by co-transformation with *ST-mRFP*, *Xylt-mRFP*, *mRFP-SYP31*, *mRFP-SYP61*, or *mRFP-VSR2* respectively (Miao et al., 2006; Delhaize et al., 2007; Tsunemitsu et al., 2018). The green and red fluorescence in a single cell were photographed at same time using laser scanning confocal microscope (CLSM, Leica, Germany).

2.6. Plant transformation, treatments, and metal content assay

The full-length coding sequence (CDS) of *PtrMTP6* was amplified from cDNA using gene specific primers (OE-PtrMTP6-F1 and OE-PtrMTP6-R1, Table S1). Then, the fragments were cloned into the plant expression vector pBI121 and driven by *Cauliflower mosaic virus* (CaMV) 35S promoter. The recombinant vector pBI121-*35S*$_{Pro}$*::PtrMTP6* was introduced into *Agrobacterium tumefaciens* strain EHA105 using the freeze-thaw method. We transformed *Populus tomentosa* using *Agrobacterium*-mediated methods as described previously (Feng et al., 2021). The transgenic poplar plants were screened on woody plant medium (WPM) containing 50 mg/L kanamycin, and the expression level of *PtrMTP6* from transgenic plants was determined via qRT-PCR. Two independent overexpressed transgenic lines were selected for treatments.

We grew the poplar saplings (including the wild type and two independent transgenic lines) for 6-weeks in a hydroponic culture, as described above. After that, the half-strength Hoagland solution was replaced by a nutrient solution supplemented with the metals of interest (5 mM $MnSO_4$ or 0.5 mM $CoCl_2$; Zhao et al., 2017; Wang et al., 2020; Wang et al. mentioned 0.1 mM Co is suitable for treatment in willow, however the plant did not show symptoms when we tried this concentration, thus we increased concentration to 0.5 mM). We kept growing the plants until symptoms were visible (2-weeks for $MnSO_4$ and 3-weeks for $CoCl_2$). The nutrient solution was replaced every three days.

We then quantified metal concentrations in the different transgenic lines of poplar and in the wildtype, after metal application. We collected and dried (65 °C for 48 h) separately the different organs of poplars (roots, stems, old leaves, mature leaves, expanding leaves, young leaves and shoot apex). About 0.05 g of dried material were digested with 4 mL HNO_3 (65%) and 1 mL $HClO_4$ (70%) at 160 °C for 3 h. After digestion, the samples were diluted to 25 mL using deionized H_2O. Metal contents of diluted liquids were then determined by ICP-MS (Aiglent, United States).

3. Results

3.1. Clone and sequence analyses of PtrMTP6

The full-length coding sequence of PtrMTP6 (XM_006386701) was successfully amplified. It encoded a deduced protein with 513 amino acids and the sequence identity with AtMTP6 is 64% (Gao et al., 2020). And the CDF signature sequence was identified in the amino acids of 117–160 (Fig. 1A). Phylogenetic analyses indicated the PtrMTP6 belongs to group 6 in the CDF family's Zn/Fe clade, which contains proteins involved in Fe transport including FieF, WmFieF and ScMMTs (Montanini et al., 2007; Gao et al., 2020).

We aligned PtrMTP6 with other proteins in the same group but from other species: AtMTP6, CsMTP6, OsMTP6, VvMTP6 and ZmMTP6 (Fig. 1A). The transmembrane topology was predicted using CCTOP (Dobson et al., 2015) and visualized by TMRPres2D (Fig. 1B). The PtrMTP6 protein shows two conserved transmembrane domains for cation efflux, each containing three predicted transmembrane helices (TMs). The PtrMTP6 protein does not contain a histidine-rich interconnecting loop between TM4 and TM5, which is different from the topology model of the classical prokaryotic CDFs (Kolaj-Robin et al., 2015). Instead, PtrMTP6 contains a histidine-rich loop between TM3 and TM4. The N-terminal domain (NTD) and C-terminal domain (CTD) of PtrMTP6 are both protruded into the cytoplasm. The CTD of MTP6 possessed a conserved zinc transporter dimerization domain (ZT-dimer). We identified the two specific motifs for the Zn/Fe group located at the putative TMII (HSVSD) and TMV (HHRAD) helixes. The H/D residues in two conserved motifs are thought to form a site for metal transport, according to the cryo-EM structure of Escherichia coli Yiip (EcFieF) (Lopez-Redondo et al., 2018).

3.2. PtrMTP6 expression confers tolerance to Mn and Co in yeast

Our previous studies demonstrated that heterologous expression of *PtrMTP6* could decrease the hypersensitivities of yeast mutant, Δ*pmr1* and Δ*cot1* to excess Mn and Co, respectively (Gao et al., 2020). To further characterize the degree of metal tolerance conferred by PtrMTP6, we compared the growth curves in yeast expressing *PtrMTP6*, relative to those in yeast transformed with an empty vector (Fig. 2). We observed that Δ*pmr1* cells expressing *PtrMTP6* grew significantly better than Δ*pmr1* cells transformed with an empty vector (Fig. 2A, *pmr1*+pYES2-PtrMTP6, *pmr1*+pYES2). However, as Fig. 2A show, the expression of *PtrMTP6* did not fully compensate for the sensitivity of Δ*pmr1* cells (*pmr1*+pYES2-PtrMTP6) as they did not approach the growth of wild-type yeast BY4741 (BY4741+pYES2). Additionally, we observed that *PtrMTP6*-expressed Δ*pmr1* cells accumulated significantly less Mn than control cells (Fig. 3A). This result suggest that PtrMTP6 confers Mn tolerance by expelling this ion from cytoplasm, however the effects of Mn accumulation and tolerance were not observed in *PtrMTP6*-expressed wild-type BY4741 cells.

In Δ*cot1*, expression of *PtrMTP6* partly confers Co tolerance in the presence of 1 mM $CoCl_2$. In addition, the expression of *PtrMTP6* also increased cell growth in the wild-type BY4741 (Fig. 2C). Furthermore, measurements of yeast metal concentrations showed that *PtrMTP6*-expressed cells showed a higher accumulation of Co than control cells, especially in Δ*cot1* cells (Fig. 3B).

3.3. Spatiotemporal patterns of PtrMTP6 transcription in different tissues

To investigate the transcript abundances of *PtrMTP6* in *Populus trichocarpa*, the mRNA levels were quantified by qRT-PCR in different organs of poplar including roots, stems, stem apex, axillary buds, mature leaves, young leaves, and petioles. The results indicate that *PtrMTP6* was expressed ubiquitously in all the examined organs (Fig. 4A). Subsequently, we further verified the organ expression profiles of *PtrMTP6* by histochemical GUS (β-glucuronidase) staining. GUS activity could be

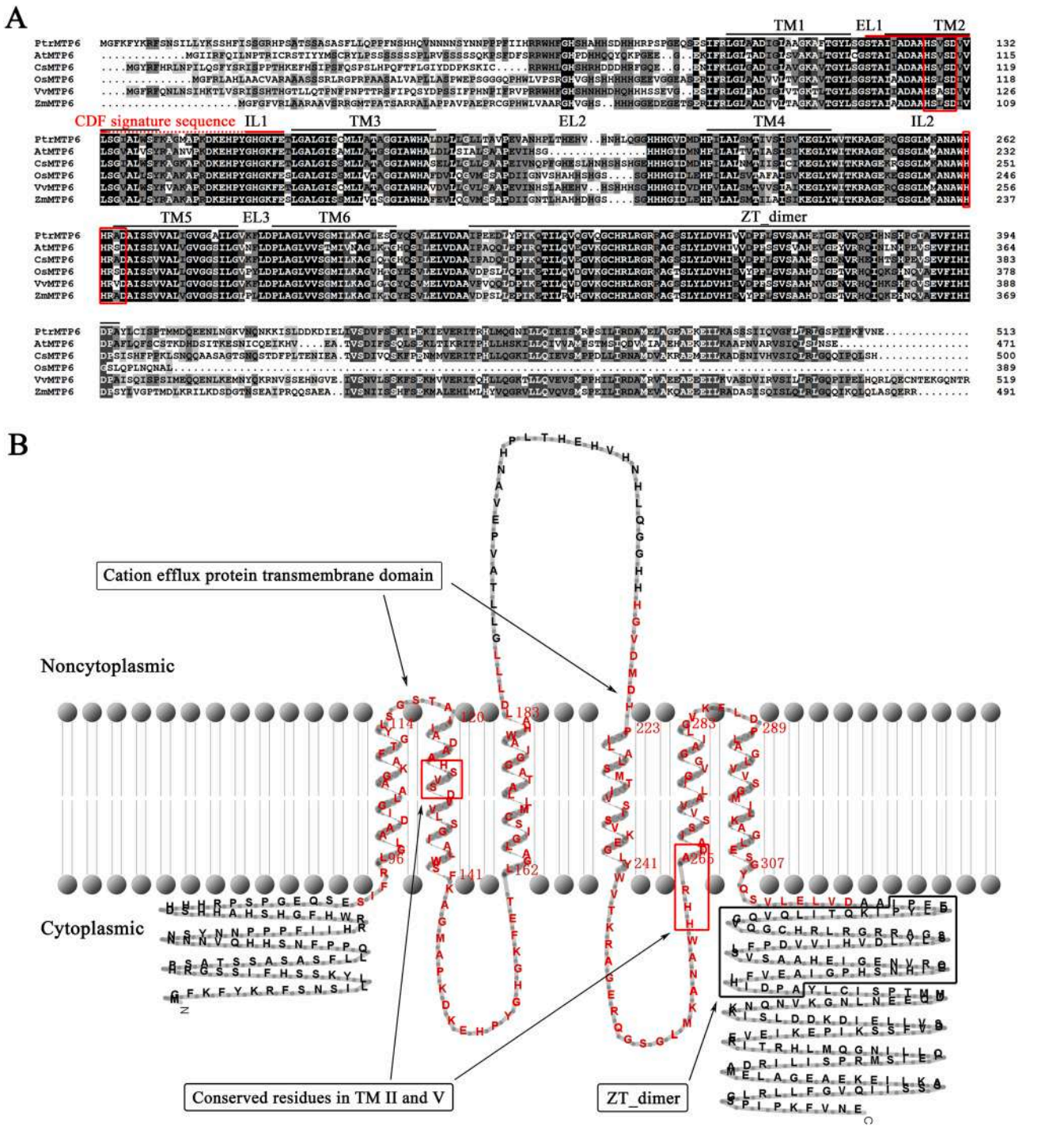

Fig. 1. Sequence analyses of PtrMTP6. (A) Multiple sequences alignment of PtrMTP6, AtMTP6, CsMTP6, OsMTP6, VvMTP6, and ZmMTP6 built by DNAMAN program. Black background, the completely conserved amino acid residues between sequences; dark gray background, conserved residues with very similar properties; gray background, conserved residues with moderately similar properties; pale gray background, conserved residues with few similar properties. TMs marked by black lines indicated the transmembrane domains predicted by CCTOP; EL, extracytosolic loop; IL intracytosolic loop; ZT-dimer marked by black lines, is the domain homologous to the zinc transporter dimerization domain; residues in red box, highly conserved residues in TM2 and TM5 related to cation binding; residues marked by red lines, the CDF signature sequence. (B) The transmembrane topology of PtrMTP6 predicted by CCTOP. Residues with red letters were conserved cation efflux protein transmembrane domain searched by InterPro. Residues in the black box were the ZT-dimer. Residues in the red box were highly conserved residues related to cation binding. For interpretation of the references to color in this figure legend, the reader is referred to the web version of this article.

detected in almost all organs (Fig. 4B-I), but there were higher expression levels in the stem phloem and in the vein of young leaves (Fig. 4D-E, G), lower expression levels in the base root, the initiation site of lateral roots and the vascular bundle of petiole (Fig. 4B-C, I). *GUS* expression was marginal in veins of mature leaves and in stem apex (Fig. 4F, H). These results indicate significant differences in the expression of *PtrMTP6* across different tissues and organs in poplar, with higher concentrations in the phloem tissue and in the vascular bundle of young leaves.

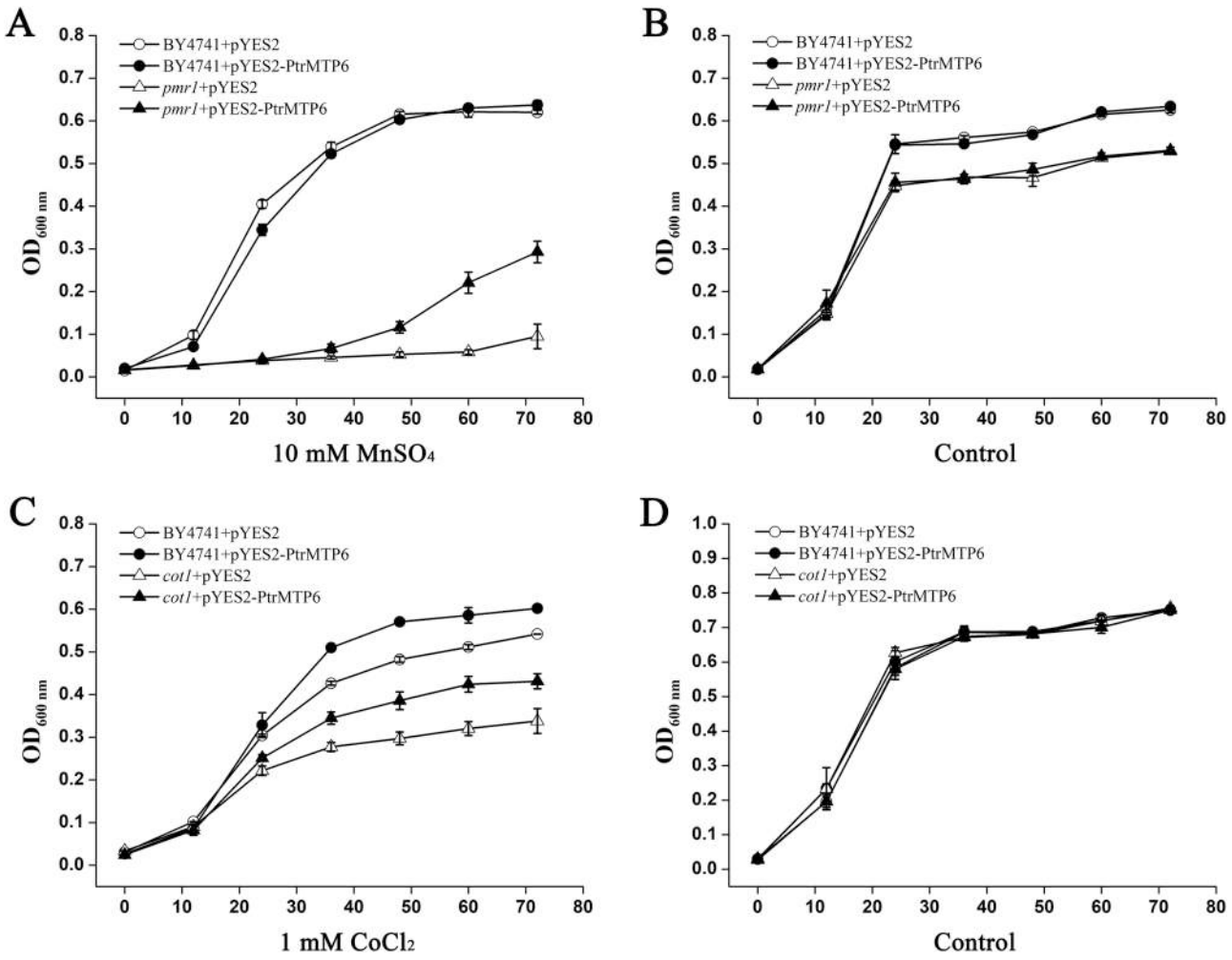

Fig. 2. Expression of *PtrMTP6* in yeast confers Mn and Co tolerance. We measure absorbance at 600 nm (OD_{600}) every 12 h to detect the yeast concentration in: (A) Yeast mutant *pmr1* and wild type BY4741 transformed with empty pYES2 vector or with *PtrMTP6* in pYES2, and cultured in the control solution(SD-Ura/Gal) with 10 mM Mn; (B) Yeast mutant *pmr1* and wild type BY4741 transformed with empty pYES2 vector or *PtrMTP6* in pYES2, and grown in the control solution; (C) Yeast mutant *cot1* and wild type BY4741 transformed with empty pYES2 vector or *PtrMTP6* in pYES2, and cultured in the control medium with 1 mM Co; (D) Yeast mutant *cot1* and wild type BY4741 transformed with empty pYES2 vector or *PtrMTP6* in pYES2, and cultured by control. Results represent mean values ± SD from three biological replicates.

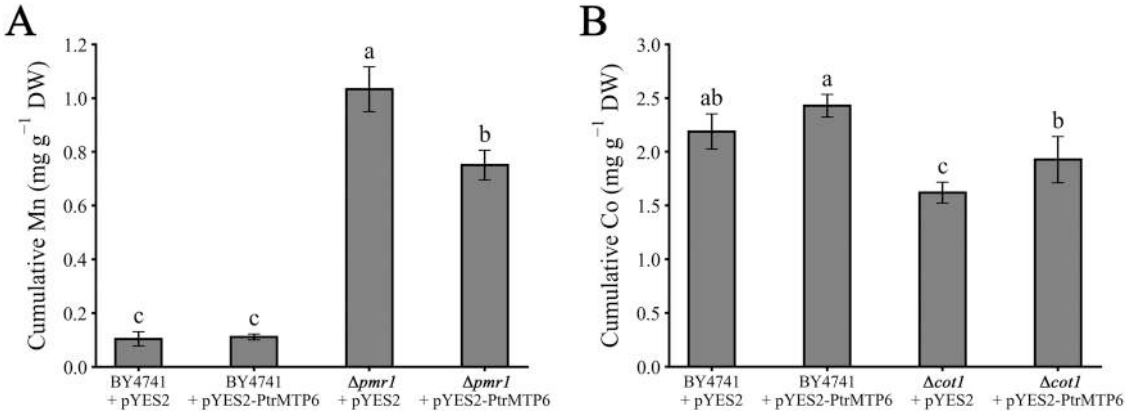

Fig. 3. The expression of PtrMTP6 affects the concentration of Mn and Co in yeast. Concentrations of (A) Mn and (B) Co in yeast cells, determined in BY4741 transformed with empty pYES2 vector, BY4741 transformed with *PtrMTP6*, *pmr1* transformed with empty pYES2 vector, and *pmr1* transformed with *PtrMTP6*. Yeasts grew in SD-Ura/Gal medium for 12 h and then with extra 5 mM Mn (in A) or with 0.5 mM Co (in B) for another 6 h. Results represent mean values ± SD from three biological replicates and different letters indicate significantly different (LSD test, $p < 0.05$).

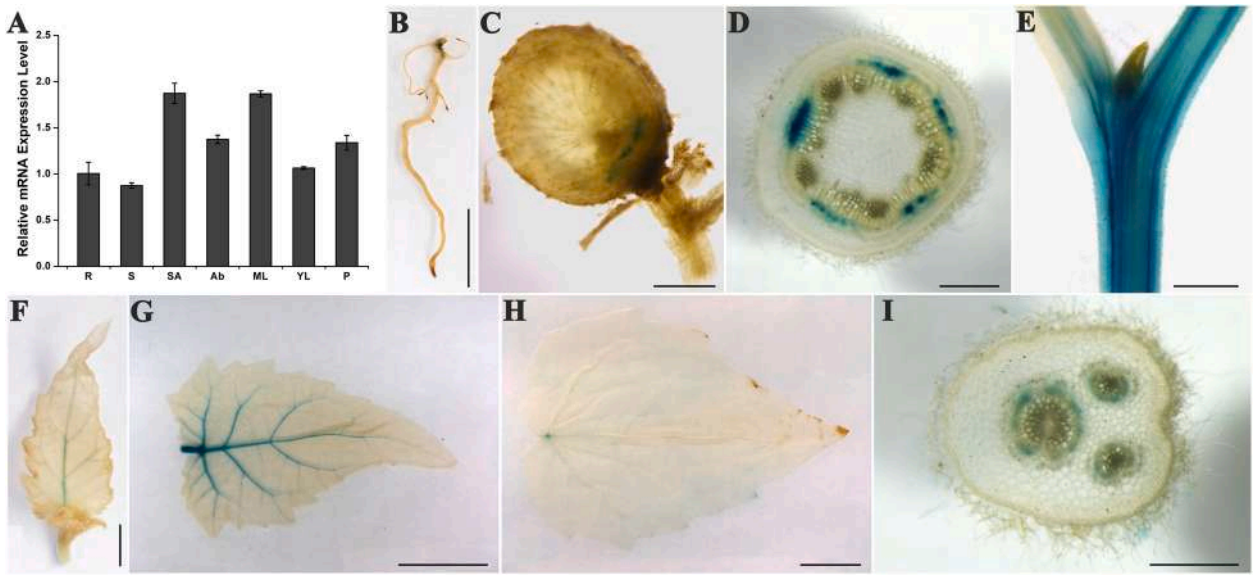

Fig. 4. Spatiotemporal patterns of *PtrMTP6* transcription. (A) The relative mRNA expression level of *PtrMTP6* in different poplar tissues detected by qRT-PCR. R, root; S, stem; SA, shoot apex; Ab, axillary bud; mL, mature leaves; YL, young leaves; P, petiole. Results represent mean values ± SD from three biological replicates. (B-I) GUS staining of root (B), root slice (C), stem slice (D), stem and axillary bud (E), shoot apex and young leaf (F), expanding leaf (G), mature leaf (H), and petiole slice (I) for $PtrMTP6_{pro}$*::GUS* transgenic lines. The scale bars were 1 cm in B, 500 μm in C, D, and I, 2 cm in E, G, and H, and 5 mm in F.

3.4. *PtrMTP6 was presented at the pre-vacuolar compartments*

To identify the subcellular localization of PtrMTP6 protein, we fused the green fluorescent protein gene (*GFP*) to the C-terminal of *PtrMTP6* and promoted it by the constitutive *Cauliflower mosaic virus* (CaMV) 35S promoter. The fused protein was transiently expressed in rice mesophyll protoplasts. Green fluorescence we observed using CLSM (Confocal Laser Scanning Microscope) and exhibited an amorphous and complex structure (Fig. 5). Further, we transiently co-expressed the *PtrMTP6-GFP* with other organelle specific markers, including *ST-mRFP* (trans-Golgi), *Xylt-mRFP* (media-Golgi), *mRFP-SYP31* (cis-Golgi), *mRFP-SYP61* (trans-Golgi network TGN), and *mRFP-VSR2* (pre-vacuolar compartments PVCs) (Fig. 5). The results indicated that most PtrMTP6-GFP signals were co-located with the red fluorescence PVC marker mRFP-VSR2 (Fig. 5E). Conversely, the signals of PtrMTP6-GFP did not coincide highly with other organelle markers (Fig. 5A-D). Indicated the PtrMTP6-GFP were presented at the vacuole sorting receptor (VSR)-marked PVCs in transgenic rice protoplasts.

3.5. *Overexpression of PtrMTP6 affects metal distribution in poplar*

We assessed the effects of PtrMTP6 protein on Mn and Co transport of by overexpressing PtrMTP6 in *Populus tomentosa*. Two independent transgenic lines carrying $35S_{Pro}$*::PtrMTP6* (OE-1 and OE-3) were confirmed by semi-qRT-PCR and qRT-PCR analysis (Fig. S1). We then grew the 6-week-old wild type (WT) and $35S_{Pro}$*::PtrMTP6* transgenic poplar plants in a hydroponic culture and they were subsequently exposed to excess Mn or Co stress. After 2 weeks of 5 mM $MnSO_4$ application, the Mn toxic symptoms started to emerge, but there was no obvious difference in Mn tolerance between wild type and transgenic lines (Fig. 6B). However, after 3 weeks of 0.5 mM $CoCl_2$ application, the growth of young leaves and shoots showed a severe inhibition in both wild type and transgenic lines, and the transgenic lines exhibited a higher level of necrotic lesion than wild type plants (Fig. 6C, D). These results indicate that the overexpression of *PtrMTP6* could increase the sensitivity of transgenic poplar to Co.

Moreover, the metal content of different organs was further analyzed. As shown in Fig. 7, although there were little phenotypic differences between transgenic lines and wild type plants under control (normal nutrient solution), the distribution of Mn and Co concentrations in different plant tissues were altered by the overexpression of *PtrMTP6* (Fig. 7A, C). Mn concentration were lower in old leaves (OL) and higher in mature leaves (mL), expanding leaves (EL), young leaves and shoot apex (YL+SA) in the control. Co concentrations were higher in young leaves and shoot apex (YL+SA) under control conditions (Fig. 7C). After application of 5 mM $MnSO_4$, we observed significant increases in Mn concentration in young leaves and shoot apex (YL+SA) in the lines overexpressing *PtrMTP6*, and lower Mn concentrations in the stem (Fig. 7B). After applying 0.5 mM $CoCl_2$, where Co concentration was higher in mature and young leaf tissues of *PtrMTP6*-overexpressed lines, relative to the wildtype, (not detected in expanding leaves (EL) for this sensitive tissue had lost its function and fall off from the plant), but Co concentrations were lower in stem. This is consistent with more obvious toxic phenotype of transgenic lines vs wild type under 0.5 mM $CoCl_2$ condition (Fig. 6C). As shown in Fig. S2, there were little differences in whole plant Mn or Co concentrations between *PtrMTP6*-overexpressed lines and the wild type plants under any treatment, indicating that PtrMTP6 does not significantly affect root Mn/Co absorption.

4. Discussion

4.1. *The PtrMTP6 protein is a Fe/Zn-CDF member, and has a similar structure with Yiip*

In plants, metal tolerance proteins (MTPs) belong to one class of CDF proteins (cation diffusion facilitator), and they have been identified ubiquitously in *Eubacteria*, *Archaea* and *Eukaryote* (Nies and Silver, 1995). Phylogenetic analyses have traditionally divided CDF members into one of three major clusters, namely Zn-CDF, Fe/Zn-CDF, and Mn-CDF respectively, depending on the substrate (Montanini et al., 2007). CDF proteins usually contain six transmembrane domains (TMs), with cytoplasmic termini and conserved residues in TM2 and TM5 (Montanini et al., 2007). The structure analysis on the CDF member YiiP in *Escherichia coli* showed that ion transported is conferred by the conformational change cycles (Lopez-Redondo et al., 2018). Yiip structure is characterized by six transmembrane helices (TMs), a Zn transport site in four-helix bundle and a dimeric structure caused by the membrane domain (Lopez-Redondo et al., 2018; Lu et al., 2009;

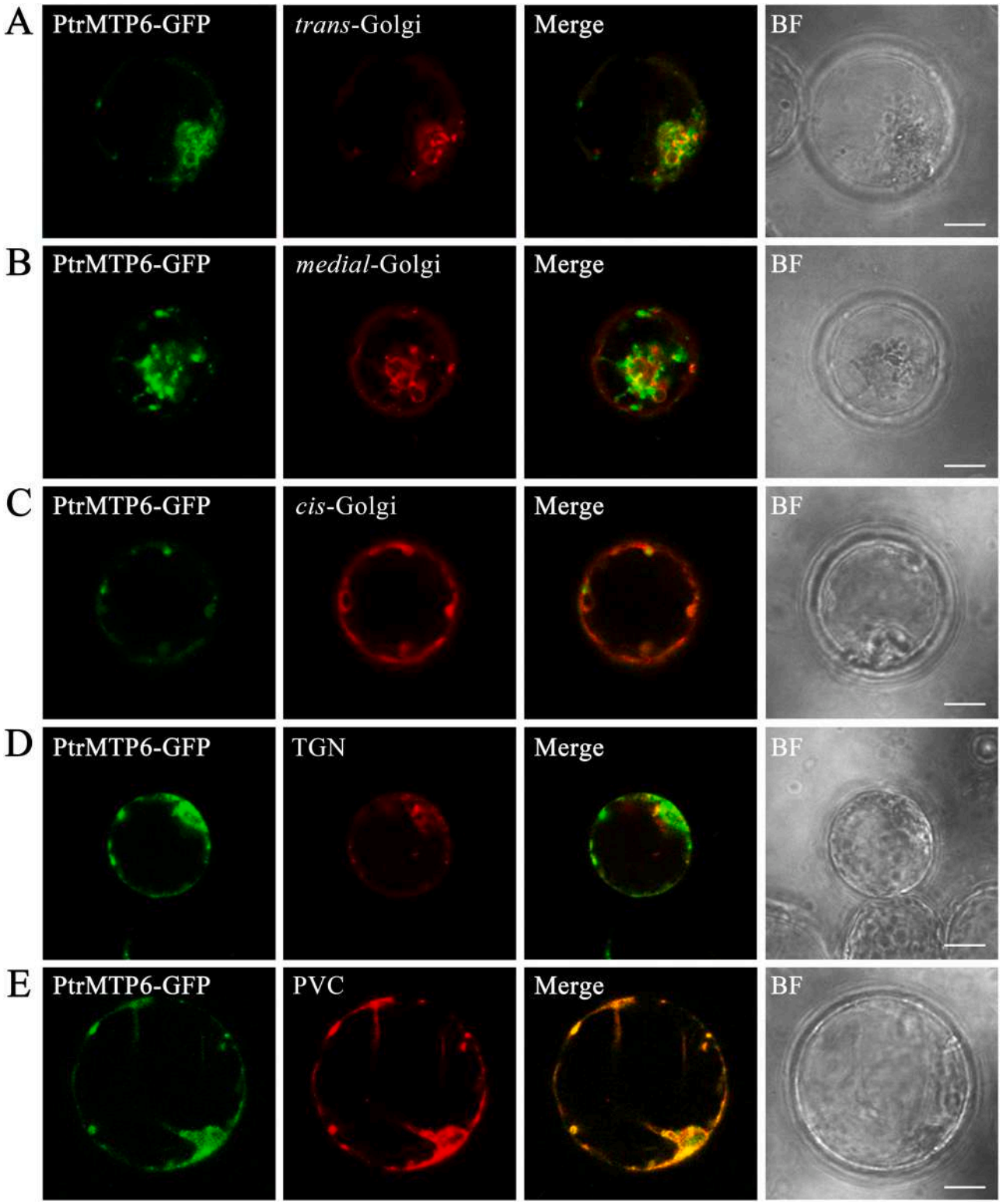

Fig. 5. PtrMTP6-GFP was presented at the pre-vacuolar compartment. The *35S$_{pro}$::PtrMTP6-GFP* and a marker construct were co-transformed into rice protoplasts, and analyzed by confocal microscopy. The first column is the green fluorescence of PtrMTP6-GFP; The second column is the red fluorescence of the markers, (A) *trans*-Golgi marked by ST-mRFP, (B) *medial*-Golgi marked by Xylt-mRFP, (C) *cis*-Golgi marked by mRFP-SYP31, (D) TGN marked by mRFP-SYP61, and (E) PVC marked by mRFP-VSR2. The third column is the result of merging the images from the first two columns, yellow colors indicate the co-localization of two signals. The fourth column is the cell under the bright field. Scale bars indicate 25 μm.

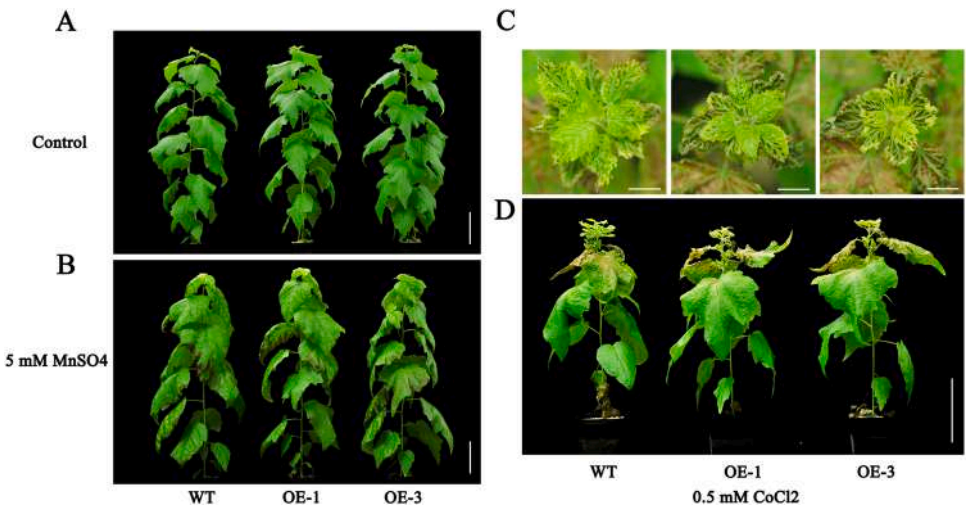

Fig. 6. The overexpression of *PtrMTP6* confers Co sensitivity. Phenotypes of the wildtype and two independent *PtrMTP6* overexpressing transgenic lines under (A) Control, (B) 5 mM $MnSO_4$ and (C and D) 0.5 mM $CoCl_2$. The scale bars are 10 cm in A, B, and D, 1 cm in C.

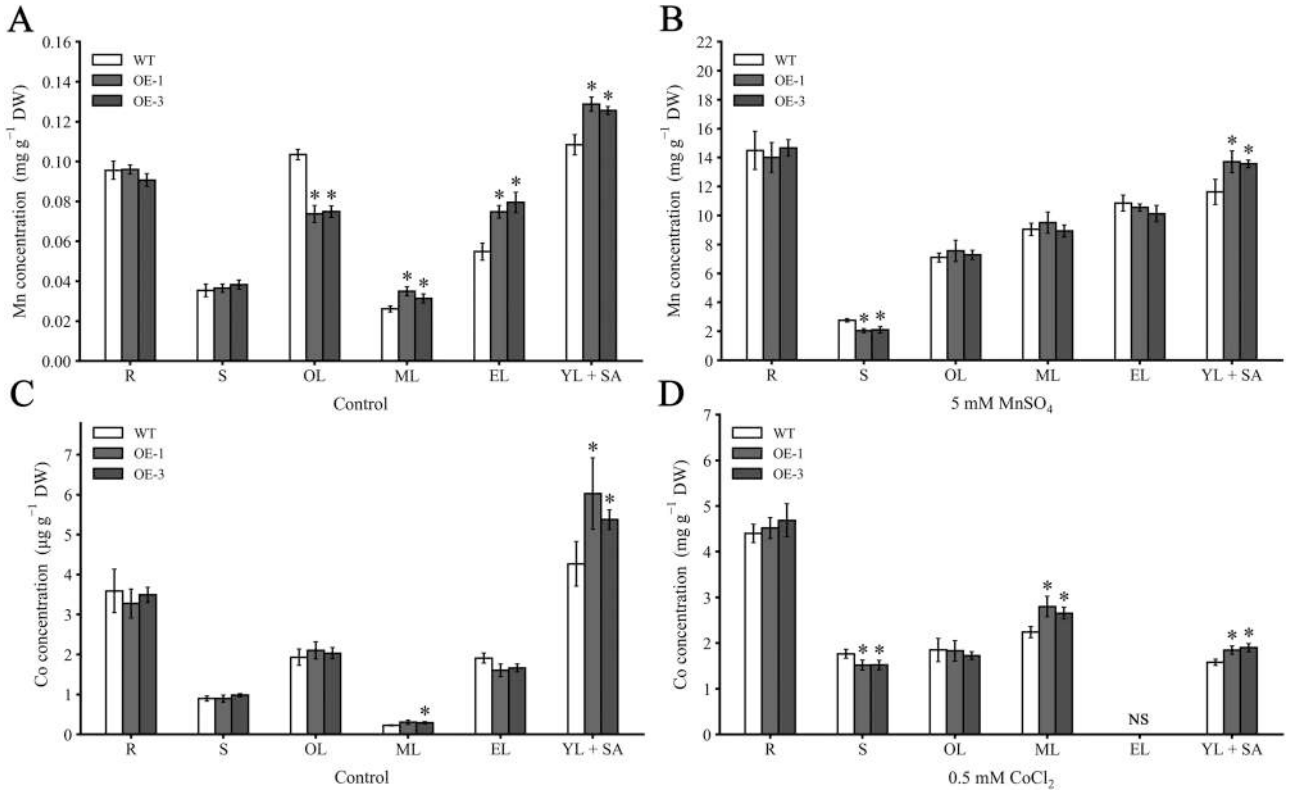

Fig. 7. Differences in Mn and Co concentrations across tissues in the wildtype and *PtrMTP6* overexpressing transgenic lines. Concentrations of Mn in (A) control treatments and (B) in response to 5 mM $MnSO_4$. Concentrations of Co (C) in control treatments and (D) in response to 0.5 mM $CoCl_2$. R, roots; S, stems; OL, old leaves; mL, mature leaves; EL, expanding leaves; YL + SA, young leaves and shoot apex. NS means meaningless results. Results represent mean values ± SD from three biological replicates, and asterisks indicate significant differences (Student's *t*-test, $p < 0.05$).

Montanini et al., 2007). Similarly, PtrMTP6 contains six transmembrane helices, a ZT-dimer (homologous with the membrane domain in Yiip) at the C-terminal domain, and constant H/D residues which are thought to form the transport site in TM2 and TM5. This similarity suggests that PtrMTP6 is also a dimeric secondary transporter driven by protons, like Yiip, and the ion transport site likely results from alternating opposite sides of the membrane by the rocking and twisting of a four-helix bundle.

4.2. The PtrMTP6 seems to transport the Mn and Co ions both into PVC

The PVC presence of PtrMTP6 was confirmed by the co-localization with the AtVSR2 protein in protoplasts. The VSR (vacuole sorting receptor) protein binds ligands in the trans-Golgi network (TGN), and transport to PVCs is then achieved via clathrin-coated vesicles (CCVs). Once in the PVCs, the VSR proteins release the ligands which are then transported to the vacuole, and then the VSR proteins turn back to TGN via vesicles (Dasilva et al., 2005). The highly relevant co-localization of

PtrMTP6-GFP and mRFP-AtVSR2 indicate that PtrMTP6 presented at the same position of VSR proteins in this process, that is PVC. This result suggested that PtrMTP6 protein seems can transport the Mn and Co ions into the PVC.

However, there have some puzzling results in yeast assay. The expression of *PtrMTP6* could remediate the hypersensitivity both of Δ*pmr1* and Δ*cot1* cells, but in wild type yeast BY4741, the expression of *PtrMTP6* only enhanced the resistance of Co (Fig. 2). Further, the expression of *PtrMTP6* decreased the Mn content of Δ*pmr1* cells but increased the Co content of Δ*cot1* cells (Fig. 3). These results seemingly suggested that the PtrMTP6 can transport Mn or Co to different places selectively. But in our opinion, this difference in the transport of Mn and Co in yeast is not caused by PtrMTP6, but by the difference between PMR1 and COT1 itself.

The PMR1 is a Ca^{2+}/Mn^{2+}-ATPase located at the Golgi apparatus and transports Mn into the Golgi apparatus, and then discharges excess Mn by exocytosis which processes sort the cargos in TGN (Keller and Simons, 1997; Lapinskas et al., 1995; Traub and Kornfeld, 1997; Dürr et al., 1998). And the COT1 is a CDF protein and located at the mitochondrial membrane and functions at the sequestering of Co into mitochondria, the studies have shown that the yeast strain increased the Co tolerance due to expression of *COT1* has an increased Co uptake (Conklin et al., 1992; Gustin et al., 2011). Clearly, although the absence of PMR1 or COT1 both confers hypersensitivity of metal in yeasts, the function of PMR1 and COT1 are not same. A key point is the PMR1 discharge excess Mn by exocytosis, but the PMR1 just transports Mn into Golgi apparatus (Lapinskas et al., 1995; Dürr et al., 1998). That means, the yeasts could discharge the Mn in Golgi apparatus even if the PMR1 is absence, the absence of PMR1 only block the Mn into Golgi apparatus from cytoplasm. We noticed that there have closely connections between PVCs and Golgi apparatus. Cargos in Golgi apparatus sorted at the TGN by receptors, the cargos for secretion then secreted, and the cargos for vacuolar were carried by clathrin-coated vesicles (CCVs) to PVC first, after that the cargos then transported to vacuole from PVC, at the same time, the receptors in PVC return by a very efficient retrograde route back to the Golgi (Dasilva et al., 2005). The VSR2 is a kind of vacuolar sorting receptor (Miao et al., 2006), and the co-located of PtrMTP6 with VSR2 suggested that the PtrMTP6 may also presence at this retrograde route and transport the Mn and Co into Golgi apparatus. In Δ*pmr1* cells, the Mn could not discharge by exocytosis due to the lack of ability of transport Mn into Golgi apparatus, this highly increased the accumulation of Mn in Δ*pmr1* cells (Lapinskas et al., 1995). When *PtrMTP6* was expressed in Δ*pmr1* cells, the PtrMTP6 may transported the Mn into PVC and further transported to Golgi apparatus by retrograde route, resulting remedy the absence of PMR1 and decreased the Mn content in yeast cells. However, in wild type yeasts, the ability of PMR1 may far surpass PtrMTP6 for transport Mn into Golgi apparatus (It may also be that the ability to discharge excess Mn by exocytosis has not increased) and masks the role of PtrMTP6, thus there is nearly no influence for Mn resistance in yeasts when *PtrMTP6* expressed (Figs. 2A, 3A). Similar results were observed in AtMTP11 protein in *Arabidopsis*, one proton-antiport Mn transporter located at the PVCs (Delhaize et al., 2007). When *AtMTP11* was expressed in Δ*pmr1*, it suppressed the Mn sensitive phenotype, but AtMTP11 did not enhance Mn tolerance of genetic background BY4743.

Different from the Mn, there is no reported researches indicated that Co has a secrete pathway similar with Mn. The yeasts could not secrete the Co even if the PtrMTP6 transported the Co into Golgi apparatus, thus the result is the sequestering of Co and increased Co accumulation in yeast (Figs. 2C and 3B). This is quite similar with COT1, the COT1 sequestered the Co into mitochondria and increased Co accumulation in yeast. Furthermore, because of the different target subcellular organelles that PtrMTP6 and COT1 compartmentalized, although the PtrMTP6 and COT1 both sequestered the Co, their function did not influence each other. Therefore, the increased tolerance or uptake of Co caused by PtrMTP6 does not seem to be related to the COT1, and could be reinforced by each other (Figs. 2C and 3B). Of course, the above hypothesis requires for further detailed experimental verification, such as accurately quantifying the Mn and Co concentration in vacuole, TGN, or PVCs, etc.

4.3. The PtrMTP6 may distribute Mn and Co to young tissues through the re-translocation of the phloem

In the previous genome-wide studies of *MTP* genes in poplar, the tissue expression levels of various *MTP* genes in *Populus trichocarpa* were determined by qRT-PCR. As shown in Fig. S3, *PtrMTP6* had the higher expression level compare with the most other members of MTPs family in poplar (Gao et al., 2020). Furthermore, the *PtrMTP6* expressed in most organs of poplar including roots, stem, stem apex, axillary bud, mature leaves, young leaves, and petiole (Fig. 4A), which is consistent with the data from the Phytozome12 transcriptome database (Gao et al., 2020). The further GUS staining showed that *PtrMTP6* was mainly expressed in the phloem tissue of stems and roots, and the vascular bundle of petioles (Fig. 4B-I). Phloem plays an important role in long-distance metal transport in plants. A previous study showed that phloem can re-translocate Cd and distribute it to other tissues, as a strategy for shoot protection (Van Belleghem et al., 2007). In the process of Fe absorption by the shoot apex and young leaves, its transport is dominated by the phloem re-mobilization after Fe transport to mature leaves via xylem, due to the immaturity of xylem structure and the low accumulated transpiration rates in these young tissues (Grusak and Dellapenna, 1999). The phloem expression of *PtrMTP6* is perhaps related with Mn/Co distribution in above-ground tissues.

Under the excess Mn stress, $35S_{Pro}$*::PtrMTP6* transgenic plants suffered the same degree of toxicity as the WT plants, while the growth of young leaves and stem apex of transgenic plants was more severely inhibited than that of the WT plants under the excessive Co stress (Fig. 6). Furthermore, the total concentration of Mn and Co of transgenic plants is not significantly different from that of the WT plants (Fig. S2). These findings indicate that PtrMTP6 may not function in the uptake or efflux of Mn and Co from soil in poplar. However, the Mn or Co concentration was significantly changed in some organs was observed in transgenic plants. In normal condition, the Mn concentration of *PtrMTP6* overexpression plants was decreased in old leaves and increased in mature leaves, expanding leaves, young leaves, and stem apex (Fig. 7A). These results suggested, that the Mn in old leaves seems was remobilization into younger tissues. The increased Co and Mn concentrations in young leaves and stem apex of transgenic lines (Fig. 7) indicated more Mn and Co accumulation in the apex. This is consistent with the more sensitive phenotype of the apex of transgenic plants under excess Co stress (Fig. 7C) and the mainly phloem expression of *PtrMTP6* (Fig. 4). Previous studies have documented that Mn toxicity appears primarily in mature tissues, while Co toxicity is more apparent in young or premature tissues (Gopal, 2014; Li et al., 2019). We confirmed this trend, and this difference of toxicity perhaps was the cause of the stem apex of transgenic plants did not show more toxic after excess Mn stress, even if the Mn accumulation was increased in the apex. Our results showed that PtrMTP6 plays an important role in the Mn/Co distribution to young tissues, but the reasons underlying this phenomenon are far from resolved.

5. Conclusion

We have functionally identified PtrMTP6, a member of group 6 in the Fe/Zn-CDFs cluster. PtrMTP6 was presented at the PVCs. Expression of *PtrMTP6* in yeast showed that PtrMTP6 functions as a metal transporter for Mn and Co. The specific expression of *PtrMTP6* in the phloem and the phenotype of $35S_{Pro}$*::PtrMTP6* transgenic plants led us to propose that PtrMTP6 is involved in the distribution of Mn and Co in poplar. Further investigation of the functions of this group of proteins may help elucidating some of the unknown processes associated with divalent cation

distribution in plants, such as Mn and Co transport into various cellular organelles. These findings provide new information for understanding the mechanism of distribution and translocation of heavy metals in plants and could facilitate the realization of the directed distribution of heavy metals in different tissues of plants, which is of great significance for limiting the distribution of heavy metals in the fruit/seed organs of grain crops and contaminated ecosystems remediation.

CRediT authorship contribution statement

Fengming Yang: Conceptualization, Methodology, Formal analysis, Investigation, Data curation, Resources, Visualization, Writing – original draft. **Yongfeng Gao:** Conceptualization, Formal analysis, Validation, Data curation, Resources, Writing – review & editing, Supervision. **Jikai Liu:** Conceptualization, Methodology, Formal analysis. **Zihao Chen:** Investigation, Formal analysis. **Víctor Resco de Dios:** Writing – review & editing. **Qian Gao:** Investigation, Formal analysis. **Meng Zhang:** Investigation, Formal analysis. **Zhuoxi Peng:** Investigation, Formal analysis. **Yinan Yao:** Resources, Writing – review & editing, Project administration, Funding acquisition.

Declaration of Competing Interest

The authors declare that they have no known competing financial interests or personal relationships that could have appeared to influence the work reported in this paper.

Acknowledgements

We express our great appreciation to Jiayi Sun at Innovative Institute of Chinese Medicine and Pharmacy, Chengdu University of Traditional Chinese Medicine, for the assistance with confocal laser scanning microscopy. This work was funded by the National Natural Science Foundation of China (31770644), Sichuan Science and Technology Program (2021YJ0508) and Sichuan International Cooperation Project (2017HH0050).

Appendix A. Supporting information

Supplementary data associated with this article can be found in the online version at doi:10.1016/j.ecoenv.2021.112868.

References

Abreu, I.A., Cabelli, D.E., 2010. Superoxide dismutases—a review of the metal-associated mechanistic variations. Biochim. Biophys. Acta-Proteins Proteom. 1804, 263–274. https://doi.org/10.1016/j.bbapap.2009.11.005.

Akkus Ozen, S., Yaman, M., 2017. Examination of correlation between histidine, sulfur, cadmium, and cobalt absorption by *morus* l., *Robinia pseudoacacia* l., and *Populus nigra* l. Commun. Soil Sci. Plant Anal. 48, 1212–1220. https://doi.org/10.1080/00103624.2017.1341913.

Andresen, E., Peiter, E., Kupper, H., 2018. Trace metal metabolism in plants. J. Exp. Bot. 69, 909–954. https://doi.org/10.1093/jxb/erx465.

Banerjee, R., Ragsdale, S.W., 2003. The many faces of vitamin b12: catalysis by cobalamin-dependent enzymes. Annu. Rev. Biochem. 72, 209–247. https://doi.org/10.1146/annurev.biochem.72.121801.161828.

Blum, M., Chang, H.Y., Chuguransky, S., Grego, T., Kandasaamy, S., Mitchell, A., Nuka, G., Paysan-Lafosse, T., Qureshi, M., Raj, S., Richardson, L., Salazar, G.A., Williams, L., Bork, P., Bridge, A., Gough, J., Haft, D.H., Letunic, I., Marchler-Bauer, A., Mi, H., Natale, D.A., Necci, M., Orengo, C.A., Pandurangan, A.P., Rivoire, C., Sigrist, C.J.A., Sillitoe, I., Thanki, N., Thomas, P.D., Tosatto, S.C.E., Wu, C.H., Bateman, A., Finn, R.D., 2021. The interpro protein families and domains database: 20 years on. Nucleic Acids Res. 49, D344–D354. https://doi.org/10.1093/nar/gkaa977.

Chang, P., Yin, H., Imanaka, T., Igarashi, Y., Li, N., Luo, F., 2020. The metal transporter crnramp1 is involved in zinc and cobalt transports in Chlamydomonas reinhardtii. Biochem. Biophys. Res. Commun. 523, 880–886. https://doi.org/10.1016/j.bbrc.2019.12.121.

Conklin, D.S., Mcmaster, J.A., Culbertson, M.R., Kung, C., 1992. Cot1, a gene involved in cobalt accumulation in Saccharomyces cerevisiae. Mol. Cell. Biol. 12, 3678–3688. https://doi.org/10.1128/mcb.12.9.3678.

Dasilva, L.L., Taylor, J.P., Hadlington, J.L., Hanton, S.L., Snowden, C.J., Fox, S.J., Foresti, O., Brandizzi, F., Denecke, J., 2005. Receptor salvage from the prevacuolar compartment is essential for efficient vacuolar protein targeting. Plant Cell 17, 132–148. https://doi.org/10.1105/tpc.104.026351.

Deetman, S., Pauliuk, S., Van Vuuren, D.P., Van Der Voet, E., Tukker, A., 2018. Scenarios for demand growth of metals in electricity generation technologies, cars, and electronic appliances. Environ. Sci. Technol. 52, 4950–4959. https://doi.org/10.1021/acs.est.7b05549.

Del Rio, L.A., Lyon, D.S., Olah, I., Glick, B., Salin, M.L., 1983. Immunocytochemical evidence for a peroxisomal localization of manganese superoxide dismutase in leaf protoplasts from a higher plant. Planta 158, 216–224. https://doi.org/10.1007/BF01075257.

Delhaize, E., Gruber, B.D., Pittman, J.K., White, R.G., Leung, H., Miao, Y., Jiang, L., Ryan, P.R., Richardson, A.E., 2007. A role for theatmtp11gene of *Arabidopsis* in manganese transport and tolerance. Plant J. 51, 198–210. https://doi.org/10.1111/j.1365-313X.2007.03138.x.

Di Lonardo, S., Capuana, M., Arnetoli, M., Gabbrielli, R., Gonnelli, C., 2011. Exploring the metal phytoremediation potential of three *Populus alba* l. Clones using an in vitro screening. Environ. Sci. Pollut. Res. 18, 82–90. https://doi.org/10.1007/s11356-010-0354-7.

Dobson, L., Remenyi, I., Tusnady, G.E., 2015. Cctop: a consensus constrained topology prediction web server. Nucleic Acids Res. 43, W408–W412. https://doi.org/10.1093/nar/gkv451.

Dürr, G., Strayle, J., Plemper, R., Elbs, S., Klee, S.K., Catty, P., Wolf, D.H., Rudolph, H.K., 1998. The medial-Golgi ion pump Pmr1 supplies the yeast secretory pathway with Ca^{2+} and Mn^{2+} required for glycosylation, sorting, and endoplasmic reticulum-associated protein degradation. Mol. Biol. Cell 9, 1149–1162. https://doi.org/10.1091/mbc.9.5.1149.

Eroglu, S., Meier, B., Von Wiren, N., Peiter, E., 2016. The vacuolar manganese transporter mtp8 determines tolerance to iron deficiency-induced chlorosis in *Arabidopsis*. Plant Physiol. 170, 1030–1045. https://doi.org/10.1104/pp.15.01194.

Feng, Q., Ou, Y., Han, Y., De Dios, V.R., Wang, L., Zhang, Q., Yao, Y., 2021. The brassinosteroid biosynthesis enzyme gene pecpd improves plant growth and salt tolerance in *Populus tomentosa*. Ind. Crops Prod. 162, 113218 https://doi.org/10.1016/j.indcrop.2020.113218.

Fischerová, Z., Tlustoš, P., Jiřina, S., Kornelie, Š., 2006. A comparison of phytoremediation capability of selected plant species for given trace elements. Environ. Pollut. 144, 93–100. https://doi.org/10.1016/j.envpol.2006.01.005.

Gao, Y., Yang, F., Liu, J., Xie, W., Zhang, L., Chen, Z., Peng, Z., Ou, Y., Yao, Y., 2020. Genome-wide identification of metal tolerance protein genes in *Populus trichocarpa* and their roles in response to various heavy metal stresses. Int. J. Mol. Sci. 21. https://doi.org/10.3390/ijms21051680.

Gietz, R.D., Schiestl, R.H., 2007. Large-scale high-efficiency yeast transformation using the liac/ss carrier DNA/peg method. Nat. Protoc. 2, 38–41. https://doi.org/10.1038/nprot.2007.15.

Gonz, Aacute, Lez, A., Lynch, J.P., 1999. Subcellular and tissue mn compartmentation in bean leaves under Mn toxicity stress. Funct. Plant Biol. 26, 811–822. https://doi.org/10.1071/pp99030.

Gopal, R., 2014. Antioxidant defense mechanism in pigeon pea under cobalt stress. J. Plant Nutr. 37, 136–145. https://doi.org/10.1080/01904167.2013.849734.

Grusak, M.A., Dellapenna, D., 1999. Improving the nutrient composition of plants to enhance human nutrition and health. Annu. Rev. Plant Physiol. Plant Mol. Biol. 50, 133–161. https://doi.org/10.1146/annurev.arplant.50.1.133.

Gustin, J.L., Zanis, M.J., Salt, D.E., 2011. Structure and evolution of the plant cation diffusion facilitator family of ion transporters. BMC Evol. Biol. 11. https://doi.org/10.1186/1471-2148-11-76.

Habib, K., Hansdóttir, S.T., Habib, H., 2020. Critical metals for electromobility: global demand scenarios for passenger vehicles, 2015–2050. Resour. Conserv. Recycl. 154, 104603 https://doi.org/10.1016/j.resconrec.2019.104603.

He, J., Li, H., Luo, J., Ma, C., Li, S., Qu, L., Gai, Y., Jiang, X., Janz, D., Polle, A., Tyree, M., Luo, Z.-B., 2013. A transcriptomic network underlies microstructural and physiological responses to cadmium in *Populus* x *canescens*. Plant Physiol. 162, 424–439. https://doi.org/10.1104/pp.113.215681.

He, J., Qin, J., Long, L., Ma, Y., Li, H., Li, K., Jiang, X., Liu, T., Polle, A., Liang, Z., Luo, Z.-B., 2011. Net cadmium flux and accumulation reveal tissue-specific oxidative stress and detoxification in *Populus* × *canescens*. Physiol. Plant 143, 50–63. https://doi.org/10.1111/j.1399-3054.2011.01487.x.

Hoagland, D.R., Arnon, D.I., 1950. The water culture method for growing plants without soil. Calif. Agric. Exp. Station Circ. https://doi.org/10.1016/S0140-6736(00)73482-9.

Horst, W.J., Fecht, M., Naumann, A., Wissemeier, A.H., Maier, P., 1999. Physiology of manganese toxicity and tolerance in *Vigna unguiculata* (l.) *walp*. J. Plant Nutr. Soil Sci. 162, 263–274. https://doi.org/10.1002/(SICI)1522-2624(199906)162:3<263::AID-JPLN263>3.0.CO;2-A.

Jefferson, R.A., 1987. Assaying chimeric genes in plants: the gus gene fusion system. Plant Mol. Biol. Rep. 5, 387–405. https://doi.org/10.1007/BF02667740.

Keller, P., Simons, K., 1997. Post-golgi biosynthetic trafficking. J. Cell Sci. 110 (Pt 24), 3001–3009. https://jcs.biologists.org/content/110/24/3001.

Kobayashi, M., Shimizu, S., 1999. Cobalt proteins. Eur. J. Biochem. 261, 1–9. https://doi.org/10.1046/j.1432-1327.1999.00186.x.

Kolaj-Robin, O., Russell, D., Hayes, K.A., Pembroke, J.T., Soulimane, T., 2015. Cation diffusion facilitator family: structure and function. FEBS Lett. 589, 1283–1295. https://doi.org/10.1016/j.febslet.2015.04.007.

Kramer, U., 2010. Metal hyperaccumulation in plants. Annu. Rev. Plant Biol. 61, 517–534. https://doi.org/10.1146/annurev-arplant-042809-112156.

Lapinskas, P.J., Cunningham, K.W., Liu, X.F., Fink, G.R., Culotta, V.C., 1995. Mutations in pmr1 suppress oxidative damage in yeast cells lacking superoxide dismutase. Mol. Cell. Biol. 15, 1382–1388. https://doi.org/10.1128/mcb.15.3.1382.

Laureysens, I., De Temmerman, L., Hastir, T., Van Gysel, M., Ceulemans, R., 2005. Clonal variation in heavy metal accumulation and biomass production in a poplar coppice culture. II. Vertical distribution and phytoextraction potential. Environ. Pollut. 133, 541–551. https://doi.org/10.1016/j.envpol.2004.06.013.

Li, J.F., Jia, Y.D., Dong, R.S., Huang, R., Liu, P.D., Li, X.Y., Wang, Z.Y., Liu, G.D., Chen, Z. J., 2019. Advances in the mechanisms of plant tolerance to manganese toxicity. Int. J. Mol. Sci. 20. https://doi.org/10.3390/ijms20205096.

Li, Z., Burow, M.D., Murai, N., 1990. High frequency generation of fertile transgenic rice plants after peg-mediated protoplast transformation. Plant Mol. Biol. Rep. 8, 276–291. https://doi.org/10.1007/BF02668764.

Livak, K.J., Schmittgen, T.D., 2001. Analysis of relative gene expression data using real-time quantitative pcr and the 2−δδct method. Methods 25, 402–408. https://doi.org/10.1006/meth.2001.1262.

Lloyd, G., Mccown, B., 1980. Commercially-feasible micropropagation of mountain laurel, Kalmia latifolia, by use of shoot-tip culture. Combined Proceedings, International Plant Propagators' Society. 30, 421–427. ⟨http://www.cabdirect.org/abstracts/19830315515.html?gitCommit=4.13.20–5-ga6ad01a⟩.

Lopez-Redondo, M.L., Coudray, N., Zhang, Z.N., Alexopoulos, J., Stokes, D.L., 2018. Structural basis for the alternating access mechanism of the cation diffusion facilitator yiip. Proc. Natl. Acad. Sci. USA 115, 3042–3047. https://doi.org/10.1073/pnas.1715051115.

Lu, M., Chai, J., Fu, D., 2009. Structural basis for autoregulation of the zinc transporter yiip. Nat. Struct. Mol. Biol. 16, 1063–1067. https://doi.org/10.1038/nsmb.1662.

Miao, Y., Pak, K.Y., Hyeran, K., Inhwan, H., Liwen, J., 2006. Localization of green fluorescent protein fusions with the seven *Arabidopsis* vacuolar sorting receptors to prevacuolar compartments in tobacco BY-2 cells. Plant Physiol. 142, 945–962. https://doi.org/10.1104/pp.106.083618.

Millaleo, R., Reyes-Díaz, M., Alberdi, M., Ivanov, A.G., Krol, M., Hüner, N.P.A., 2013. Excess manganese differentially inhibits photosystem i versus ii in *Arabidopsis thaliana*. J. Exp. Bot. 64, 343–354. https://doi.org/10.1093/jxb/ers339.

Mohanty, N., Vass, I., Demeter, S., 1989. Impairment of photosystem 2 activity at the level of secondary quinone electron acceptor in chloroplasts treated with cobalt, nickel and zinc ions. Physiol. Plant 76, 386–390. https://doi.org/10.1111/j.1399-3054.1989.tb06208.x.

Montanini, B., Blaudez, D., Jeandroz, S., Sanders, D., Chalot, M., 2007. Phylogenetic and functional analysis of the cation diffusion facilitator (cdf) family: Improved signature and prediction of substrate specificity. BMC Genom. 8. https://doi.org/10.1186/1471-2164-8-107.

Nies, D.H., Silver, S., 1995. Ion efflux systems involved in bacterial metal resistances. J. Ind. Microbiol 14, 186–199. https://doi.org/10.1007/BF01569902.

Palit, S., Sharma, A., Talukder, G., 1994. Effects of cobalt on plants. Bot. Rev. 60, 149–181. https://doi.org/10.1007/BF02856575.

Peiter, E., Montanini, B., Gobert, A., Pedas, P., Husted, S., Maathuis, F.J.M., Blaudez, D., Chalot, M., Sanders, D., 2007. A secretory pathway-localized cation diffusion facilitator confers plant manganese tolerance. Proc. Natl. Acad. Sci. USA. 104, 8532. https://doi.org/10.1073/pnas.0609507104.

Pietrini, F., Zacchini, M., Iori, V., Pietrosanti, L., Bianconi, D., Massacci, A., 2009. Screening of poplar clones for cadmium phytoremediation using photosynthesis, biomass and cadmium content analyses. Int. J. Phytoremediat. 12, 105–120. https://doi.org/10.1080/15226510902767163.

Spyropoulos, I.C., Liakopoulos, T.D., Bagos, P.G., Hamodrakas, S.J., 2004. Tmrpres2d: high quality visual representation of transmembrane protein models. Bioinformatics 20, 3258–3260. https://doi.org/10.1093/bioinformatics/bth358.

Traub, L.M., Kornfeld, S., 1997. The trans-golgi network: a late secretory sorting station. Curr. Opin. Cell Biol. 9, 527–533. https://doi.org/10.1016/S0955-0674(97)80029-4.

Tsunemitsu, Y., Genga, M., Okada, T., Yamaji, N., Ma, J.F., Miyazaki, A., Kato, S.-I., Iwasaki, K., Ueno, D., 2018. A member of cation diffusion facilitator family, mtp11, is required for manganese tolerance and high fertility in rice. Planta 248, 231–241. https://doi.org/10.1007/s00425-018-2890-1.

Umena, Y., Kawakami, K., Shen, J.-R., Kamiya, N., 2011. Crystal structure of oxygen-evolving photosystem ii at a resolution of 1.9 Å. Nature 473, 55–60. https://doi.org/10.1038/nature09913.

Unterbrunner, R., Puschenreiter, M., Sommer, P., Wieshammer, G., Tlustoš, P., Zupan, M., Wenzel, W.W., 2007. Heavy metal accumulation in trees growing on contaminated sites in central europe. Environ. Pollut. 148, 107–114. https://doi.org/10.1016/j.envpol.2006.10.035.

Van Belleghem, F., Cuypers, A., Semane, B., Smeets, K., Vangronsveld, J., D'haen, J., Valcke, R., 2007. Subcellular localization of cadmium in roots and leaves of *Arabidopsis thaliana*. New Phytol. 173, 495–508. https://doi.org/10.1111/j.1469-8137.2006.01940.x.

Woo, E.-J., Dunwell, J.M., Goodenough, P.W., Marvier, A.C., Pickersgill, R.W., 2000. Germin is a manganese containing homohexamer with oxalate oxidase and superoxide dismutase activities. Nat. Struct. Biol. 7, 1036–1040. https://doi.org/10.1038/80954.

Wang, Y.M., Yang, Q., Xu, H., Liu, Y.J., Yang, H.L., 2020. Physiological and transcriptomic analysis provide novel insight into cobalt stress responses in willow. Sci. Rep. 10, 2308. https://doi.org/10.1038/s41598-020-59177-y.

Zhao, J., Wang, W., Zhou, H., Wang, R., Zhang, P., Wang, H., Pan, X., Xu, J., 2017. Manganese toxicity inhibited root growth by disrupting auxin biosynthesis and transport in *Arabidopsis*. Front. Plant Sci. 8, 272. https://doi.org/10.3389/fpls.2017.00272.